J Electr Eng Technol.2015; 10(2): 595-602
http://dx.doi.org/10.5370/JEET.2015.10.2.595

ISSN(Print) 1975-0102
ISSN(Online) 2093-7423

A Novel Wound Rotor Type for Brushless Doubly Fed Induction Generator

Xin Chen† and Xuefan Wang*

Abstract – The rotor configuration of the brushless doubly fed induction generator (BDFIG) plays an important role in its performance. In order to make the magnetomotive force (MMF) space vector in one set rotor windings to couple both magnetic fields with different pole-pair and have low resistance and inductance, this paper presents a novel wound rotor type for BDFIG with low space harmonic contents. In accordance with the principles of slot MMF harmonics and unequal element coils, this novel rotor winding is designed to be composed of three-layer unequal-pitch unequal-turn coils. The optimal design process and rules are given in detail with an example. The performance of a 700kW 2/4 pole-pair prototype with the proposed wound rotor is analyzed by the finite element simulation and experimental test, which are also carried out to verify the effectiveness of the proposed wound rotor configuration.

Keywords: Brushless doubly fed induction generator (BDFIG), Wound rotor, Slot MMF harmonics, Unequal element coils

1. Introduction

Brushless doubly-fed induction generator (BDFIG), regarding to be an alternative of doubly-fed induction generator (DFIG), has gained broad appeal to be ideal future generators in wind turbines. The advantages of the BDFIG-based wind turbines includes eliminating brush and slip rings, lower operation and maintenance fees, taking fractional rated capacity of converters and superior crowbarless fault ride-through (FRT) capability [1-3]. Owing to these clear superiorities, the commercial potential of BDFIG is enormous.

In order to couple both of the two magnetic fields between two stator windings in BDFIG, some configurations of specific rotor winding types have been proposed in the literatures. A cage-type rotor of the BDFIG, which is known as the "nested-loop", was originally proposed and investigated by Broadway and Burbridge [4]. To reduce the rotor spatial harmonics, a novel cage rotor configuration comprising loops connected in series was presented in [5], and it was shown that the rotor harmonics have a direct impact on the referred rotor leakage reactance and the effective performance of the machine. Compare with the conventional wound rotor windings, large cage-type rotor winding designs are deemed to create higher space harmonic contents. A comparison analysis of nested-loop rotor windings and series-loop wound rotor winding was presented in [6]. Focus on the electrical and manufacturing, it shows the latter may be preferable to large machines, but they did not propose methods to reduce harmonic content which cannot be ignored for BDFIG.

The purpose of this paper is to present the general method to design a wound rotor winding for BDFIG. Moreover, the rules to reduce the harmonic content are also given. In this paper, a double-layer unequal element coils wound rotor structure of the BDFIG is presented to reduce the harmonic contents and improve the winding factors. A detailed analysis and design principles of the proposed rotor winding is given in section 2. Thereafter, an analytical model is given to calculate the proposed unequal element coil in section 3. Optimization and selection of winding elements is implemented base on this model. On the basis of previous analysis, both simulations and experimental results are presented to illustrate the performance of a prototype with the proposed rotor winding type in section 4. Experimental testes were implemented on a D560 frame-size 700kW 2/4 pole-pair wound rotor BDFIG.

2. Winding Design

The stator of BDFIG has two independent windings. In general, stator winding 1 acts as an electrical terminal for directly generating power and is therefore named as the power winding (PW). For another, stator winding 2, named as the control winding (CW), acts as an electrical terminal to connect with a variable voltage variable frequency converter which owns only a partial rated power capacity. These two stator windings can be distinguish

† Corresponding Author: State Key Laboratory of Advanced Electromagnetic Engineering and Technology, Huazhong University of Science and Technology, China.(chenxin_hust@163.com)
* State Key Laboratory of Advanced Electromagnetic Engineering and Technology, Huazhong University of Science and Technology, China.
Received: June 18, 2014; Accepted: October 24, 2014

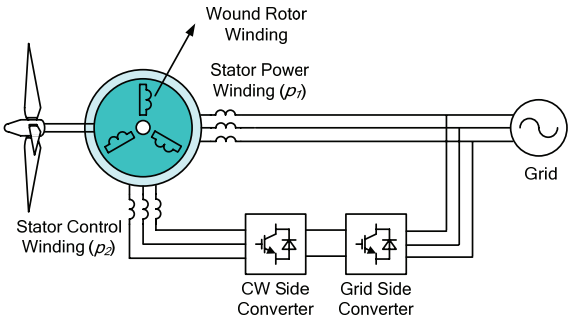

Fig. 1. Wind turbine system based on BDFIG

from each other in pole pairs for generating two fundamental magnetic fields. The number p_1 and p_2 represent the pole-pair of PW and CW respectively. A BDFIG-based wind turbine system is shown in Fig. 1.

The rotor of the BDFIG is required to be designed to couple both of the two magnetic fields, p_1 and p_2, which were generated by the two windings in the stator. However, the other order of harmonic contents in rotor winding (RW) should be as little as possible. Due to any order of harmonic except for p_1 and p_2 will not induce voltage in the stator, from the BDFIG standpoint, it manifests as harmonic reactance.

Approximately, the relation of the air gap peak flux densities for two fundamental, $B_{\delta 1}$ and $B_{\delta 2}$, is given by [4]

$$\frac{B_{\delta 1}}{B_{\delta 2}} = \frac{p_1 k_{Nr2}}{p_2 k_{Nr1}} \tag{1}$$

where k_{Nr1} and k_{Nr2} are the winding factors for two fundamental in RW. This is a critical operation rule of BDFIG and it indicates that the winding factors of two fundamental, p_1 and p_2, have a inherent relation with the relevant two air gap flux densities, therefore, the design goal of the RW is to achieve high winding factors for two fundamentals and low winding factors for other harmonics.

With the above conclusion in mind, we should set constraints for the design optimizations of the RW firstly. They are: (1) the winding factors of p_1 and p_2 pole-pair both should be above 0.7; (2) the resultant MMF percent of the highest harmonic content should be kept less than 3%. These constraints are obtained considering the performance of the initial design models and the previous prototypes.

2.1 Theory of slot MMF harmonics

In practical induction machines, the coils of the windings are always placed in slots along with the air gap. Unless the winding distribution is sinusoidal, under the action of currents, the polyphase windings will create a fundamental MMF with a wide range of harmonics. The harmonic contents with $v=kZ/p\pm1=2kmq\pm1$ (k=1, 2, 3,…) orders are the slot MMF harmonics, and Z is the number of slots, m is the number of the phases, p and q is the number of pole-pair and slots per pole per phase respectively. All slot MMF harmonics have the same distribution factor with the fundamental, so they may not be destroyed [7].

In the following analysis, it must to clarify that only space harmonics on account of distributed winding are included, while permeance harmonics on account of slotting effects will be intentionally ignored. In practice, the geometrical profile of the air gap, rather than the size and arrangement of the coils, determines the permeance harmonics. Based on the same consideration, harmonics due to magnetic field saturation effect are also ignored.

For the v-th order slot MMF harmonic,

$$\begin{aligned} f_{Av} &= F_{\phi v}\cos v\theta\cos\omega t \\ f_{Bv} &= F_{\phi v}\cos(v\theta-2\pi/3)\cos(\omega t-2\pi/3) \\ f_{Cv} &= F_{\phi v}\cos(v\theta-4\pi/3)\cos(\omega t-4\pi/3) \end{aligned} \tag{2}$$

where f is the 3-phase MMF generated by the A-, B- and C-phase currents, θ is the angular displacement, ω is the angular speed and t is the time.

When v=1, the resultant MMF of the fundamental is,

$$f_1(t,\theta) = \frac{3}{2}F_{\phi 1}\cos(\omega t-\theta) \tag{3}$$

When v=2mq-1, the resultant MMF of v-th harmonic is,

$$f_v(t,\theta) = \frac{3}{2}F_{\phi v}\cos\left[\omega t+(2mq-1)\theta\right] \tag{4}$$

Comparing (3) and (4), it is shown that the rotating direction of v=2mq-1-th slot MMF harmonic is reverse with that of the fundamental. As shown in Fig. 2, voltage phasor diagrams for three-phase symmetrical winding with Z=6, p_1=2 and p_2=4 are given. The first order slot MMF harmonic for p_1 pole-pair is $v=2$, which is also the fundamental component for p_2 pole-pair. Meanwhile, the first order slot MMF harmonic for p_2 pole-pair is v=0.5, which is also the fundamental component for p_1 pole-pair.

Summarize the analysis above: (1) The MMFs of p_1 pole-pair and p_2 pole-pair appear simultaneously; (2) the MMFs rotating directions of p_1 pole-pair and p_2 pole-pair are reverse; (3) The winding factors of p_1 pole-pair and p_2 pole-pair are the same.

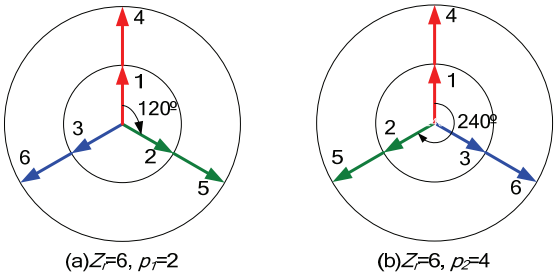

Fig. 2. Voltage phasor diagrams for (a) Z_r=6, p_1=2 and (b) Z_r=6, p_2=4

In consideration of the basic operation rule of the BDFIG, the RW should have the ability to generate two opposite rotating MMFs which also differ in pole-pair. By using the principle of slot MMF harmonic, the design of the RW can satisfy the rotor structure requirement of the BDFIG and the number of the rotor slots should be choose as,

$$Z_r = p_1 + p_2 \tag{5}$$

2.2 Method of slot-number phasor diagram

The phase distribution of the induced electromotive force (EMF) for each coil sides is illustrated with a voltage phasor diagram in Fig. 2, which is presented in electrical degrees and is an effective tool to analysis winding [8]. However, it is cumbersome to draw the voltage phasor diagram with a large number of slots. In this paper, a new analysis method, slot-number phasor diagram, is adapted to explain the design process of the RW in BDFIG. The slot-number phasor diagram develops as an imaginary process of "cutting" and "unrolling" the rotary voltage phasor diagram to a linear counterpart.

The three-phase coils for the RW with Z=6, p_1=2 and p_2=4, which mentioned above, can be found from the slot-number phasor diagrams as Fig. 3 shown. The slot numbers demonstrate the space vectors of the EMFs or MMFs produced by the coils (or the upper layer coils) inserted in the slots, the sign "–" in front of the slot numbers demonstrate the reverse polarity coils (or the upper layer coils) in 360 electric degrees.

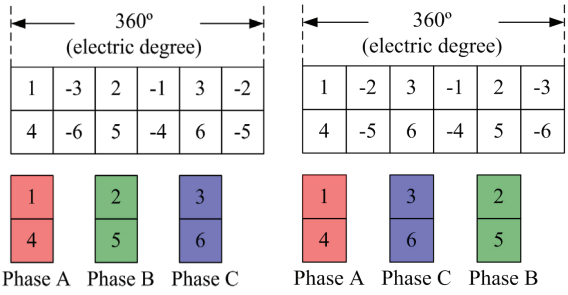

(a)Z_r=6, p_1=2 (b)Z_r=6, p_2=4

Fig. 3. Slot-number phasor diagrams for (a) Z_r=6, p_1=2 and) Z_r=6, p_2=4

2.3 Slot division and discard

According to (5), when p_1=2 and p_2=4, the number of the rotor slots Z_r should be chosen as 6 (named as Case 1), however, an amount of MMFs harmonic contents except for that of p_1 pole-pair and p_2 pole-pair still exists. Since less rotor slots leads to a relatively high referred rotor harmonic leakage inductance, consequently, next step should be taken to effectively expand the number of slots. In order to maintain the MMFs of p_1 pole-pair and p_2 pole-pair appear simultaneously, an integral multiple of Z_r could be adopted and expressed as following,

$$Z_r = k*(p_1 + p_2) \tag{6}$$

where k is a positive integer. The number of the rotor phase m_r should be deliberately designed to $(p_1+p_2)/m_k$, where m_r and m_k also should be positive integers. The slot-number phasor diagram of Z_r=84 and p_1=2 is plotted as shown in Fig. 4, make a comparison with Fig. 3, the number of the rotor phase is 6, the slot number in each phase seems to be divided to 14 (named as Case 2).

After slot division, we should discard some usefulness coils in the next step. Taking phase A1 for example, firstly, we should discard some coils which exceed 180 electrical degrees in the slot-number phasor diagram. As shown in Fig. 5, slot 12, 13 and 14 exceed the boundary of the 180 electrical degrees in the slot-number phasor diagram with p_2 pole-pair (The winding arrangement after this step was named as Case 3). Secondly, in order to improve the winding factor of the two fundamentals, slot-number 9 and 10 can be discarded. At this moment, the slot-number of phase A1 is constituted of 1, 2, 3, 4, 5, 6, 7, 8 and 9 (named as Case 4).

The proportional relation of the fundamental resultant MMF and v-th harmonic resultant MMF that created by m_r-phase symmetrical currents can be expressed as [7],

$$\frac{F_{\varphi v}}{F_{\varphi 1}} = \frac{p_1 k_{Nv}}{p_v k_{N1}} \tag{7}$$

where p_v and k_{Nv} is the pole-pair and winding factor for v-th harmonic, respectively. To analyze the above cases,

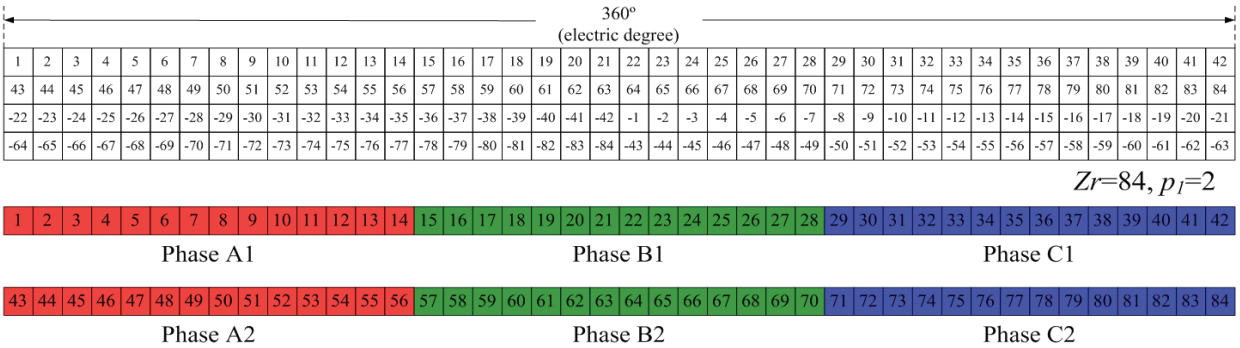

Fig. 4. Slot-number phasor diagram for describing slot division (Z_r=84, p_1=2)

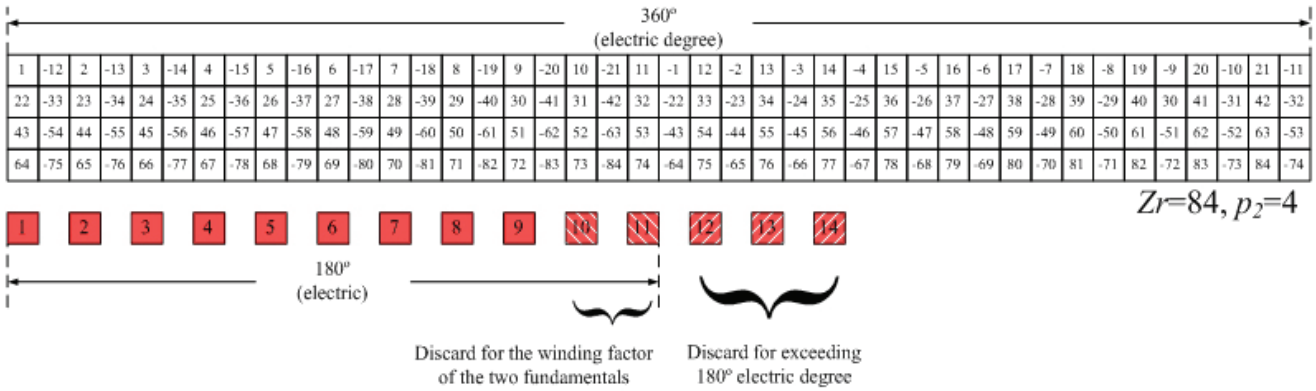

Fig. 5. Slot-number phasor diagram for describing slot discard (Z_r=84, p_2=4)

Table 1. Winding harmonic analysis of Case 1~Case 4

Pole pairs	Case 1		Case 2		Case 3		Case 4	
	Winding factor	Resultant MMF (%)	Winding factor	Resultant MMF (%)	Winding factor	Resultant MMF (%)	Winding factor	Resultant MMF (%)
2	0.8660	-200.00	0.6068	-293.22	0.6537	-215.54	0.6796	-187.52
4	0.8660	+100.00	0.4139	+100.00	0.6065	+100.00	0.7248	+100.00
8	0.8660	-50.00	0.0313	-3.77	0.0069	-0.56	0.0244	-1.68
10	0.8660	+40.00	0.1399	+13.52	0.1699	+11.20	0.0559	+3.08
14	0.8660	-28.57	0.0619	-4.27	0.0455	-2.14	0.1111	-4.38
16	0.8660	+25.00	0.0324	+1.95	0.0140	+0.57	0.0455	+1.56
20	0.8660	-20.00	0.0847	-4.09	0.1158	-3.81	0.0660	-1.82
22	0.8660	+18.18	0.0308	+1.35	0.0166	+0.49	0.0499	+1.25
26	0.8660	-15.38	0.0715	-2.65	0.1005	-2.54	0.0801	-1.70

the winding factors and the resultant MMFs calculated from (7) are shown in Table 1, where signs "+" and "–" represent the opposite rotation of the resultant MMFs in forward direction and reverse direction. Make a comparison with Case 1 to Case 4, the effect of the above design processes is obvious. Case 4 can basically satisfy the design requirements of RW as shown in Table 1, but at the same time some harmonic contents are still high and will affect the performance.

3. Optimal Design by Unequal Element Coils

In this section, to guarantee the better performance of the machine, the winding arrangement was optimal design by unequal-pitch unequal-turn coils, which is also called unequal element coils as Fig. 5 shown. The goal of the optimization is to make the space harmonic content as less as possible and the MMF space vector of a phase winding along with the air gap close to sinusoidal distribution by choosing and regulating the coil turns and coil pitches reasonably. An analytical model is given hereinafter to calculate and choose the unequal element coils.

For a general winding with unequal element coils, the number of coils with N_1 turns is c_1, the number of coils with N_2 turns is c_2, the vector sum of all the coil electrical potentials for phase A1 can be expressed as,

$$F_{Av} = N_1(1-e^{-jy_1\alpha v})(1+e^{-j\alpha v}+\ldots+e^{-jc_1\alpha v}) + N_2 e^{-jc\alpha v}(1-e^{-jy_2\alpha v})(1+e^{-j\alpha v}+\ldots+e^{-jc_2\alpha v}) \quad (8)$$

where y_1 and y_2 is the short pitch of the two element coils, respectively; c_1 and c_2 is the number of upper conductors for the two element coils, c is the pitch between them, respectively; v is the harmonic order; α is the slot pitch, which is $2\pi/84$ in this example. The complex numbers are used to represent the phase differences. The winding factor of the v-th harmonic of the unequal element coils can be express as,

$$k_{wv} = \frac{|F_{Av}|}{2c_1N_1 + 2c_2N_2} \quad (9)$$

Using the introduced winding factor, the harmonic spectra of the MMF of unequal element coils can be investigated.

The pole pitches of p_1 pole-pair and p_2 pole-pair are,

$$\tau_1 = \frac{Z_r}{2p_1} = \frac{84}{2*2} = 21,\ \tau_2 = \frac{Z_r}{2p_2} = \frac{84}{2*4} = 10.5 \quad (10)$$

To enlarge the winding factors of p_1 pole-pair and p_2 pole-pair and lessen the winding factors of the other harmonic, y_1 and y_2 should be set in the range of τ_1 and τ_2, pitch y_1 was set to 12. Meanwhile, the size of the slot

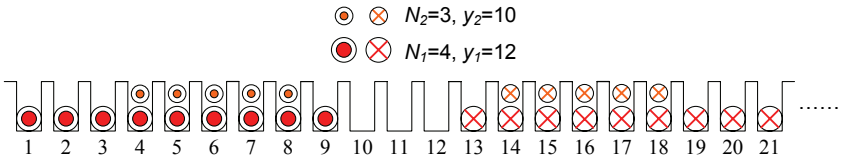

Fig. 6. Winding arrangement for unequal element coils of phase A1

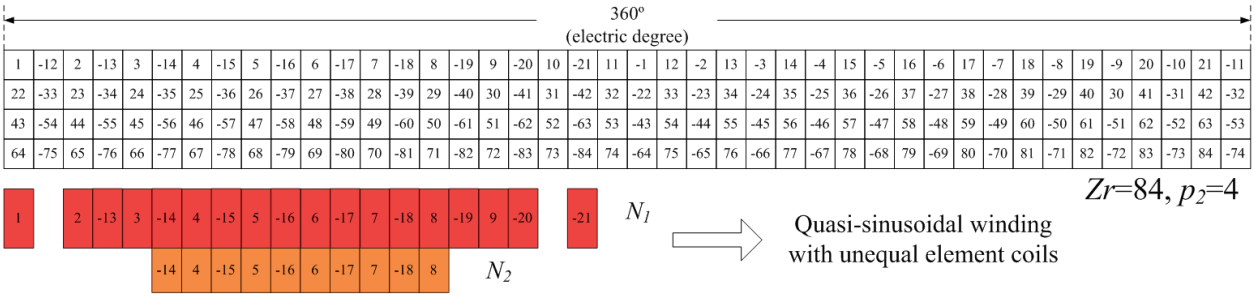

Fig. 7. Slot-number phasor diagram for unequal element coils of phase A1 (Zr=84, p_2=4)

Table 2. Winding harmonic analysis of Case 4 and Case 5

Pole pairs	Case 4		Case 5	
	Winding factor	Resultant MMF (%)	Winding factor	Resultant MMF (%)
2	0.6796	-187.52	0.7072	-184.19
4	0.7248	+100.00	0.7679	+100.00
8	0.0244	-1.68	0.0204	-1.33
10	0.0559	+3.08	0.0401	+2.08
14	0.1111	-4.38	0.0509	-1.89
16	0.0455	+1.56	0.0897	+2.92
20	0.0660	-1.82	0.0236	-0.61
22	0.0499	+1.25	0.1035	+2.45
26	0.0801	-1.70	0.0255	-0.51

should be considered, the layer of the RW has better to be limited to three-layer, therefore pitch y_2 was set to be 10.

The coil turns of the two element coils, N_1 and N_2, are needed to be calculated and regulated by using the design program according to (8) and (9). In this paper, the turns of the two element coils were set to be 4 and 3. The winding arrangement of phase A1 was describe in Fig. 5 (named as Case 5). In the slot-number phasor diagram, when the upper and lower conductors were both represented, the MMF produced by the unequal element coils was a good match for quasi-sinusolidal distribution as Fig. 6 shown. The comparison of winding factors and the resultant MMFs before and after optimization was shown in Table 2, Case 5 satisfies the design requirements and had been chosen to implement in the prototype.

4. Results and Discussion

The winding configuration proposed and analyzed hereinbefore is applied to design of a 700kW 2/4 pole-pair wound rotor BDFIG. The cross-section of the rotor type is shown in Fig. 7, which will be used to demonstrate the performance with a finite element (FE) method.

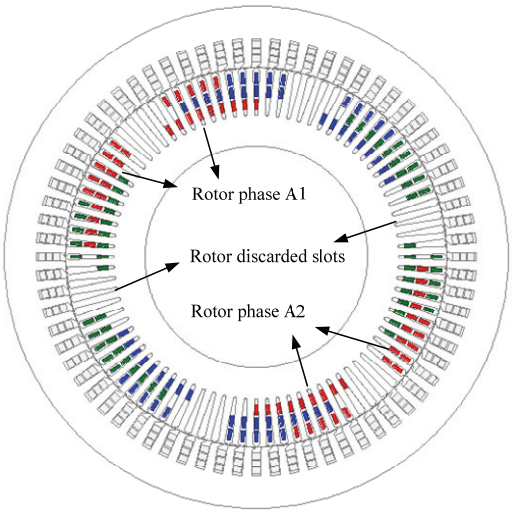

Fig. 8. BDFIG cross-section with proposed rotor winding. Different colors are used to distinguish rotor three-phase

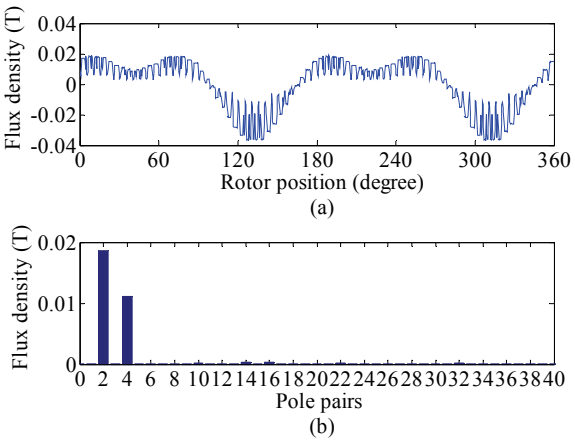

Fig. 9. Diagrams obtained from magneto-static FE simulation (a) Air-gap flux density (b) relevant space harmonic spectra

To calculate and analyze the air gap flux density in the proposed RW structure, a magneto-static FE simulation is built firstly to present a no-load operating condition. Only the three-phase RW are energized with the currents:

$$i_a = 1A, i_b = -0.5A, i_c = -0.5A \quad (11)$$

The obtained air gap density with the corresponding harmonics spectrum is provided in Fig. 8. There is a good agreement between the space harmonic spectra from magneto-static FE simulation and that from the predictions in Table 2.

A 2-D time-harmonic field application analysis is carried out later to model the BDFIG and study the air gap magnetic fields. The design parameters and main dimensions of the prototype are listed in Table 3. The flux lines of the generator are shown in Fig. 9. In line with (1), the flux density of 4 pole-pair is nearly twice as large as that of 2 pole-pair. It is predicted that the magnetic fields of 4 and 2 pole-pair are induced in the RW simultaneously to ensure that the magnetic fields generated by two stator windings are indirect coupling.

It is worth comprising the electromagnetic performance of each winding configurations. Fig. 11 compare the values of the predicted flux linkage for the winding configurations, it is clear that Case 5 has the maximum flux linkage, this means that the rotor winding of Case 5 obtain more cross coupling than other cases. The torque curves for the four winding configurations are presented in Fig. 12. It can be seen that Case 5 has the highest value of output torque and the lowest value of ripple torque.

The experiments have been implemented on a 700kW

Table 3. Main machine dimensions

Description	Value	Description	Value
Length of air gap	1.6 mm	Rotor ID	420 mm
Stator OD	950 mm	Stator ID	720 mm
Stator slot number	72	Rotor slot number	84
Stator slot width	17.8 mm	Rotor slot width	10.8 mm
Stator slot depth	54 mm	Rotor slot depth	71 mm
Stator teeth width	13.6 mm	Rotor teeth width	16.3 mm
PW pole-pair	2	CW pole-pair	4
Rated voltage	450 V	Rated frequency	60 Hz
PW connection	delta	CW connection	delta
Rotor type	wound	Frame size	D560

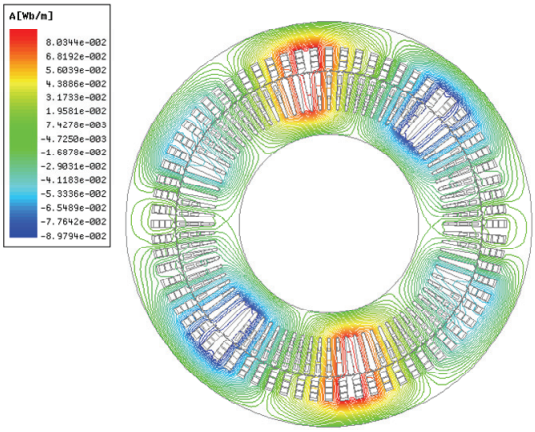

Fig. 10. Flux distributions in time-harmonic FE simulation of the prototype BDFIG

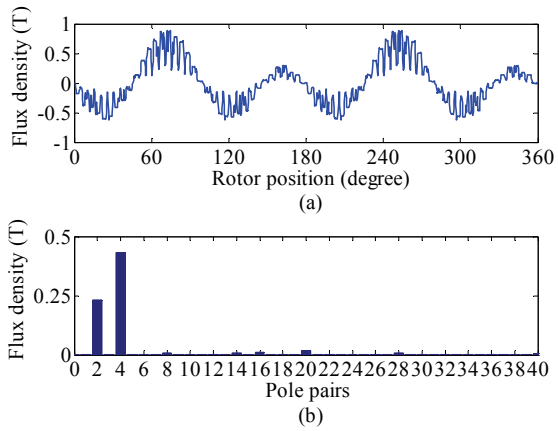

Fig. 11. Diagrams obtained from time-harmonic FE simulation: (a) Air gap flux density; (b) relevant space harmonic spectra

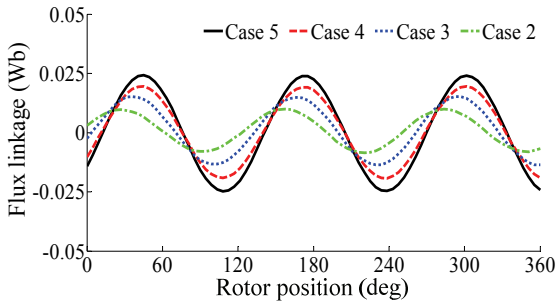

Fig. 12. Comparison of the rotor winding flux linkage for each winding configurations

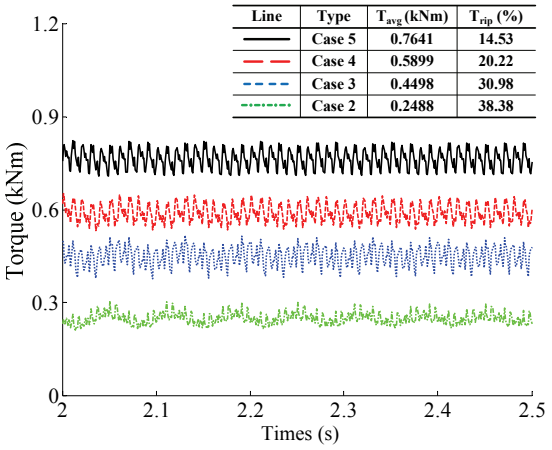

Fig. 13. Comparison of torque curves for each winding configurations (T_{avg} is the average torque and T_{rip} is the peak to peak value of the torque ripple divided by T_{avg})

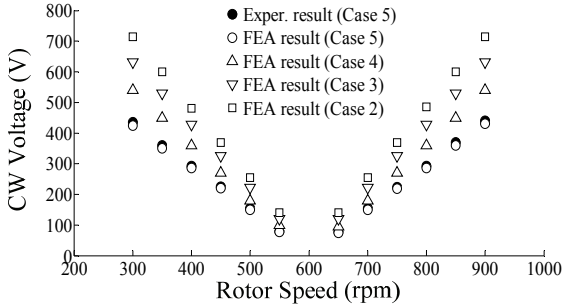

Fig. 14. CW excited voltage against rotor speed (the induced voltage of the open circuited PW is 450Vrms, 60Hz)

(a) D-560 frame size prototype BDFIG

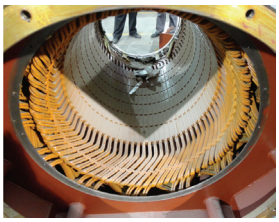

(b) stator

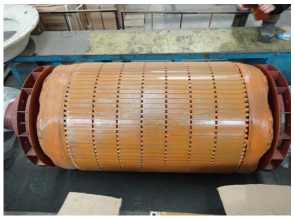

(c) rotor

Fig. 15. Pictures of the proposed wound rotor BDFIG

prototype BDFIG as Fig. 14 shown. The CW is supplied with a three-phase converter, while the PW is in open circuit situation and measured by a voltmeter. The PW induced voltage was kept at 450Vrms/60Hz, the CW excited voltage was regulated with the rotor speed and PW voltage. The FE calculated and experimental measured CW voltage versus rotating speed for the prototype BDFIG is presented in Fig. 13. It is evident that, intermediate the stator two windings, the optimized winding arrangement (Case 5) owns a more sufficient ability for creating cross coupling.

Before the proposed wound rotor type BDFIG construction, the most widely used type is the nested-loop cage rotor BDFIG which makes a great contribution to BDFIG analysis [2-6]. The nested-loop cage rotor contains multiple loops and can be regarded as a concentrated winding, thus, it is difficult to obtain high winding factors for both two pole pairs. Under the conditions of the consistent rotor slot area, the consistent number of rotor conductors and excited by the same value current, compare with the nested-loop cage rotor, the proposed wound rotor BDFIG will obtain higher copper usage efficiency due to the higher winding factors of the two pole pairs.

Another issue is the copper loss. Compared with the same size BDFIG with nested-loop cage rotor, the higher value of the referred rotor resistance for wound rotor may leads to higher rotor copper losses [7]. Nonetheless, large reduction of the rotor harmonics and the referred rotor leakage inductance are more effective in improving performance of the generator and counteracts the negative influence of the increased rotor copper loss.

From the viewpoint of manufacture and generator performance, the specially fabricated nested-loop cage rotor is made of copper alloys and brass, which needs more manufacturing complexity and higher cost, and this special welded construction also needs safety evaluation for wind turbines. In addition, the bars of the nested-loop cage rotor must be insulated which is hard to cast. However, the manufacturing process required for the proposed wound rotor type BDFIG is as straightforward as the traditional wound rotor DFIG design. It dose not change much, except for needing two types of coils with different number of turns. Therefore, upgrading the production line from DFIG to wound rotor type BDFIG is very convenient for wind turbines manufacturers.

5. Conclusion

The space harmonics of air gap flux density has a strong impact on the performance of a BDFIG. Based on slot MMF harmonic principle and unequal element coils, a low space harmonic content wound rotor type BDFIG is described for the first time in this paper. The proposed wound rotor with unequal element coils shows a good performance and the manufacturing process required for the proposed wound rotor BDFIG construction is similar with the traditional wound rotor DFIG design. Hence, this research has significant meaning in advancing the commercial use of BDFIG in wind turbines.

Acknowledgements

This work was supported by the China National Key Technology Support Program (No. 2012BAG03B01).

References

[1] Polinder, H.; Ferreira, J.A.; Jensen, B.B.; Abrahamsen, A.B.; Atallah, K.; McMahon, R.A., "Trends in Wind Turbine Generator Systems," Emerging and Selected Topics in Power Electronics, IEEE Journal of, vol. 1, no. 3, pp. 174,185, Sept. 2013.

[2] McMahon, R.A.; Roberts, P.C.; Wang, X.; Tavner,

P.J., "Performance of BDFM as generator and motor," Electric Power Applications, IEE Proceedings - , vol. 153, no. 2, pp. 289,299, 2 March 2006.

[3] T. Long, S. Shao, P. Malliband, E. Abdi, and R. A. McMahon, "Crowbarless fault ride through of the brushless doubly fed induction generator in a wind turbine under symmetrical voltage dips," IEEE Trans. Ind. Electron., vol. 60, no. 7, pp. 2833-2841, Jul. 2013.

[4] Broadway, A. R. W., and L. Burbridge. "Self-cascaded machine: a low-speed motor or high-frequency brushless alternator." Proceedings of the Institution of Electrical Engineers. Vol. 117. No. 7. Jul. 1970.

[5] Gorginpour, H.; Jandaghi, B.; Oraee, H., "A novel rotor configuration for brushless doubly-fed induction generators," Electric Power Applications, IET, vol. 7, no. 2, pp. 106,115, Feb. 2013.

[6] McMahon, R.; Tavner, P.; Abdi, E.; Malliband, P.; Barker, D., "Characterising brushless doubly fed machine rotors," Electric Power Applications, IET , vol. 7, no. 7, pp. 535, 543, Aug. 2013.

[7] Boldea, Ion. The induction machines design handbook. CRC press, 2009.

[8] Lipo, Thomas A. Introduction to AC machine design. Wisconsin Power Electronics Research Center, University of Wisconsin, 2004.

Xin Chen He was born in Jingzhou, China, on February 17, 1989. He received the Bachelor's degree from Huazhong University of Science and Technology (HUST), in 2010. He is presently pursuing the Ph.D. degree at HUST. His researches include wound rotor brushless doubly-fed machine design and control.

Xuefan Wang He was born in Wuhan, China, on December 26, 1954. He received the Ph.D. degree in electrical engineering from Huazhong University of Science and Technology, China, in 1989. He is presently a Professor in the same university. His research interests include electrical machines and power electronics, particularly for wound rotor brushless doubly-fed machine design and application.